"PORE PRESSURE PREDICTION METHODS USING NORMAL COMPACTION TREND BASED ON SEISMIC INVERSION "

Lei Ting[1,2,*], Yin Xing-Yao[1,2] and Zong Zhao-Yun[1,2]

[1] School of Geosciences, China University of Petroleum (Huadong), Qingdao, China

[2] Laboratory for Marine Mineral Resources, Qingdao National Laboratory for Marine Science and Technology, Qingdao, Shandong, China

ABSTRACT

Pore pressure prediction plays an important role in hydraulic fracturing. The pore pressure in shale cannot be directly measured but to be inferred by the normal velocity trend, so methods based on the effective stress theory are dedicated to establishing a function between seismic interval velocity and pore pressure. Among them the mostly used is Eaton's equation. However, how to precisely quantify the state of compaction remains unsolved. In this study, the AVO/AVA simultaneous inversion was introduced to estimate P-velocity. According to the exponential relationship between the pore pressure and the ratio of normal compaction acoustic transit time to the measured, three methods based on Eaton's equation were proposed for shale gas pore pressure, respectively. The fitting method avoids the estimation of the normal compaction trend (NCT) by the fitted nonlinear relationship between borehole-side pore pressure (inferred by the Eaton's equation) and P-velocity. The direct calculation method directly estimates the NCT with the linear trend line (LTL). Whereas the model-based calculation method constructs the NCT model using the NCT transit time well logs obtained by the LTL. The result shows that the approach of estimating the NCT impacts the pore pressure both on the accuracy and the horizontal continuity significantly, which implicates that the constraint between traces must be taken into account when computing the NCT, as well as lithology.

1. INTRODUCTION

Shale gas usually has the characteristic of high pore pressure [Serebryakov et al., 2002]. Pressure prediction plays an important role in hydraulic fracturing, as well as reducing the risks of drilling hazards. It has been studied that the main mechanisms of abnormal high pore pressure are compaction disequilibrium (under-compaction) and hydrocarbon generation [Gutierrez, Braunsdor, and Couzens, 2006]. The primary depositional setting for under-compaction is dominantly delta and the lithology is mainly shale [Law and Spencer, 1998]. Under-compaction is caused by the rapidly subside sediments in basins, in this case the fluids in pores could only be partially expelled when the formation has extremely low permeability. The remained fluids in pores have to support part of the weight of overlying sediments and so produce abnormal high pressure. Besides, porosity in this case is higher than the normal. But it has been confirmed [Meissner, 1981; Tissot, 1984] that the increase of porosity can be caused by hydrocarbon generation as well, which is more likely to be in gas-bearing shale. Sonic velocities observed by acoustic log is lower than it is thought to be with higher porosity and this change is mainly controlled by the amount of compliant porosity [Sviridov, Mayr and Shapiro, 2017]. The difference between the sonic measures and the

theoretical velocities is used for the pore pressure prediction. The theoretical velocity is generally called as normal velocity trend, which indicates the normal compaction trend (NCT).

In pore pressure prediction, NCT is used to compute the difference between the measures and the theoretical values, and the pore pressure can be predicted by this difference. Zhang [2011] has reviewed fracture gradient prediction methods and the commonly used empirical methods. Methods based on the effective stress theory [Hubbert and Rubby, 1959] are dedicated to establishing a relationship between seismic interval velocity and pore pressure [Fillippone, 1982]. In fact, other physical parameters are used as well, like resistivity [Eaton, 1972]. So accurate seismic interval velocity is needed for the estimate of pore pressure. On the point of this, there have been some researches for high precision velocity. Hong [2008] used neural network inversion to gain wave impedance, and extracted interval velocity by Gardner formula. Despite this, there remains a need for an efficient method that can precisely quantify NCT. Han et al. [2017] simulated the P- and S-velocities using the clay-plus-silt (CPS) model to gain normal velocity trend, and then completed the pore pressure prediction with Eaton's equation. The result was good.

Getting the proper NCT is a hard work, not only the knowledge to a field is needed for the determination of the coefficient, but also repeated attempts are performed to gain satisfied results. In this case, we tried to find a way to avoid the direct computation of NCT. In this study, AVO/AVA simultaneous inversion was performed to gain accurate seismic interval velocity. Then, the fitting method which avoids the NCT by the fitting formula, the direct calculation method which directly computes the NCT, and the model-based calculation method which estimates the NCT by constructing the NCT model, were proposed to predict shale gas pore pressure. Lastly, the effect of the NCT generated by different methods on the result can be seen from comparative analysis.

2. EATON'S EQUATION

Pore pressure was first predicted by the equivalent depth method [Hottman and Johnson, 1965], which was based on NCT only considered under-compaction and the error would be very large if there existed other mechanisms. Forster [1966] analyzed the feasibility and the existent problems of pore pressure prediction. Eaton [1975] summed up the work of former researchers and proposed Eaton's equation to settle the problem that the predicted pore pressure didn't match the measures well when only under-compaction was considered in geologically complicated basins. The stratigraphic factors, diagenetic processes, stratigraphic assemblage conditions and other genetic mechanisms were took into account. It was actually an empirical method and the empirical coefficient required a lot of logging data to determine.

Adapted Eaton's methods depend on the NCT, and pore pressure can either be predicted by electrical resistivity or sonic velocity. When using velocity, NCT can be estimated by the linear trend line (LTL) [Peter, Richard, and Peter, 2004; Tingay et al., 2009]:

$$\ln(\Delta t_n) = \ln(\Delta t_0) - C_1 H \tag{1}$$

Where Δt_n is normal acoustic transit time at the depth of H, Δt_0 is surface acoustic transit time, and C_1 is compaction coefficient which is determined by several attempts referring to transit time well logs. Pore pressure prediction equation is:

$$P_p = P_o - \left(P_o - P_n\right)\left(\frac{\Delta t_n}{\Delta t_s}\right)^{C_2} \tag{2}$$

Where: P_p is pore pressure, Mpa; P_0 is overburden pressure, Mpa; P_n is normal compaction pore pressure, Mpa; C_2 is the region exponent relates to overpressure formation mechanisms. In this studied area, a value of 2.0 is taken based on the calibration work with actual pressure data; Δt_n is the normal compaction acoustic transit time, $\mu s/m$; Δt_s is measured acoustic transit time, $\mu s/m$.

Borehole-side pore pressure was calculated by Eaton's equation using well logs. The NCT contributes to the pore pressure significantly and the impact can be evidently seen in this process (Figure 1). In Figure 1 (a), the NCT was estimated on Well A and B disregarding the lithology, so the gradient C_1 of the LTL was taken as 0.0001 for Well A and 0.00007 for Well B and were kept the same from the start to end. The pore pressures were presented next to the NCTs. In Figure 1 (b), different lithology was considered. On the acoustic transit time logs, the sudden change implicates the change of lithology. The lithology underneath the sudden change in the depth range of 3284 to 3580m on Well A is dominantly mudstone and shale, while the lithology in the depth range of 3163 to 3283m on Well B is dominantly mudstone. The gradients C_1 were 0.00005 and 0.00016 on Well A for the two parts, and C_1 were 0.00008 and 0.00006 on Well B. The result shows that NCT impacts both
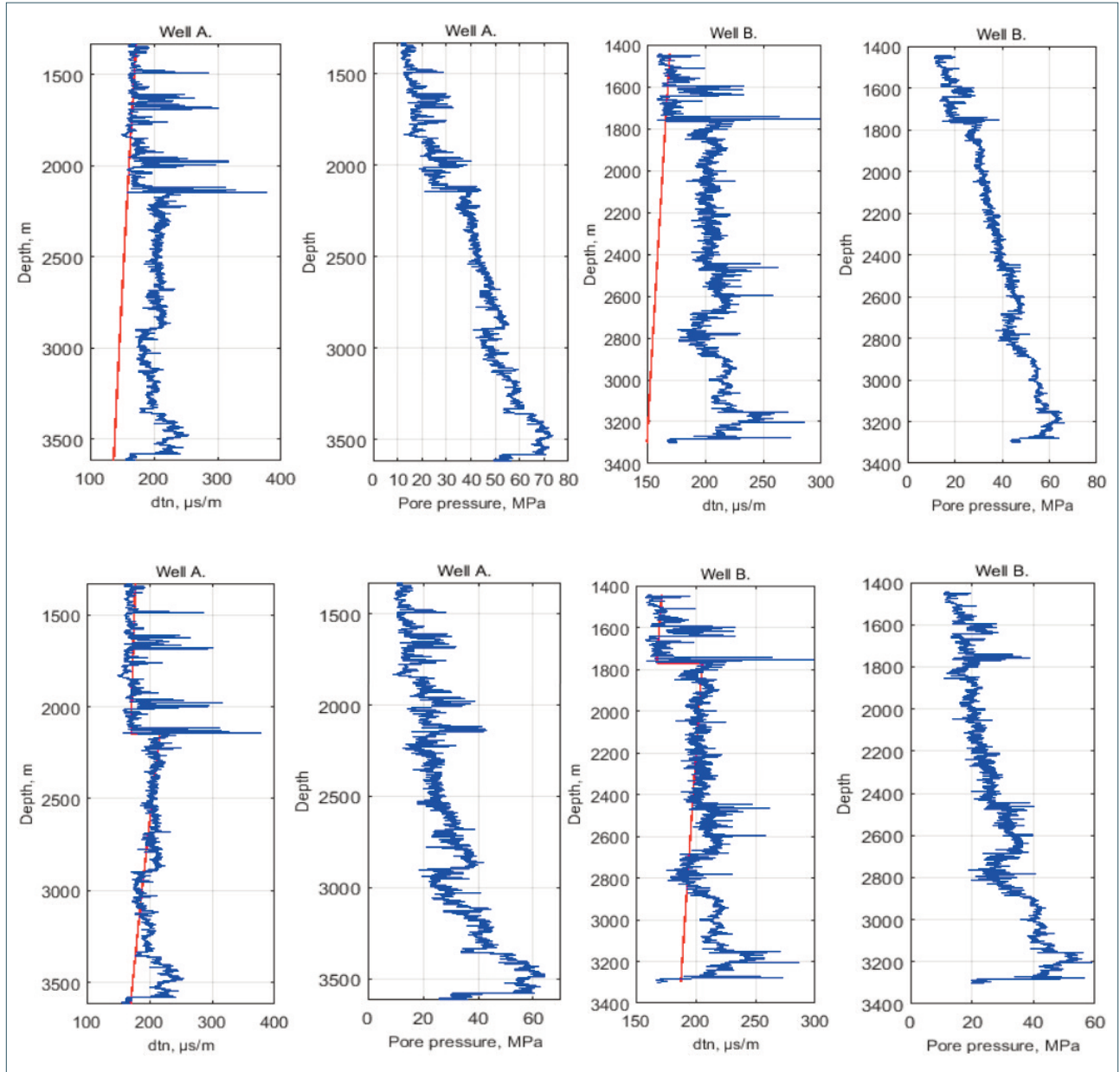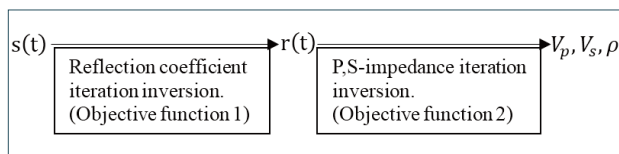
FIGURE 1. (a) Estimation of NCT on Well A and B disregarding lithology. The gradient C_1 is 0.0001 on Well A and 0.00007 on Well B. (b) Estimation of NCT on Well A and B considering lithology. The gradients C_1 are 0.00005 and 0.00016 on Well A, and 0.00008 and 0.00006 on Well B. Estimation of NCT on Well A and B in the case of disregarding and considering lithology. The red lines are NCT (Δt_n), and the blue lines are well log Δt_s and pore pressure P_p. The pore pressure gradient in (b) is smaller than that of (a). The maximum pressure values of (b) are lower than (a). When estimating the NCT by LTL, lithology must be considered to gain more reasonable results.

value and trend. Compare the pore pressure on Well A in Figure 1 (a) and (b), the maximum value of (b) is lower, and the decrease reaches to 7Mpa. The pressure in (b) shows more details due to the larger difference at the adjacent depth. Besides, the pressure gradient in (b) is smaller than that of (a). It is more reasonable to consider lithology that different lithology gets different background Δt_s, so the gradient C_1 needs to be carefully determined to identify the overpressure zone. Overpressure zone is the area where $\Delta t_s > \Delta t_n$.

3. AVO/AVA SIMULTANEOUS INVERSION

3.1 THEORY

Prestack inversion techniques use seismic angle stacks which contain rich amplitude information and can effectively improve the ability of lithology and fluid characterization [Li et al., 2007]. AVA simultaneous inversion can be divided into two steps: reflectivity with sparse spike inversion and P-, S-wave impedance and density with simultaneous inversion [Yang, 2010; Yuan et al., 2015; Zong et al., 2017]. This is performed as follows:

```
s(t) ──────────────►r(t)──────────────►V_p, V_s, ρ
     ┌─────────────────┐ ┌─────────────────┐
     │ Reflection coefficient │ │ P,S-impedance iteration │
     │ iteration inversion.   │ │ inversion.              │
     │ (Objective function 1) │ │ (Objective function 2)  │
     └─────────────────┘ └─────────────────┘
```

Reflectivity is inverted by sparse spike inversion. Sparse spike inversion [Debeye and RIEL, 1990] assumes that large reflectivities are sparse, and they are superimposed on a series of small reflectivities that corresponds to Gaussian distribution. Initial reflectivity is estimated by maximum-likelihood deconvolution. Then the optimal reflectivity can be found by minimizing the objective function 1[Wang et al., 2006]:

$$F = L_p(r) + \lambda L_p(s-d) \tag{3}$$

Where r is reflectivity, d is recorded seismic data, s is synthetic seismic data, λ is residual weight factor, and p,q are norm factors. The lower λ is, the more sparse r is. A low λ emphasizes the sum of the reflectivity is small and will result in little details. A high λ emphasizes the residual of seismic data is small and will result in more details.

P-, S-wave impedance and density are inverted by simultaneous inversion. Refer to the model-based poststack inversion [Russell and Hampson, 1991], the reflectivity is:

$$R_{pi} \approx \frac{1}{2}\frac{\Delta Z}{Z} = \frac{1}{2}\Delta \ln Z = \frac{1}{2}(\ln Z_{i+1} - \ln Z_i) \tag{4}$$

Written in matrix form is:

$$\begin{bmatrix} R_{p1} \\ R_{p2} \\ \vdots \\ R_{p(N-1)} \end{bmatrix} = \begin{bmatrix} -0.5 & 0.5 & 0 & \cdots & 0 & 0 \\ 0 & -0.5 & 0.5 & \cdots & 0 & 0 \\ \vdots & \vdots & \vdots & \vdots & \vdots & \vdots \\ 0 & 0 & 0 & \cdots & -0.5 & 0.5 \end{bmatrix} \begin{bmatrix} L_{Ip1} \\ L_{Ip2} \\ \vdots \\ L_{IpN} \end{bmatrix} \tag{5}$$

$$R_p = DL_{Ip} \tag{6}$$

Where N is the number of the layers, R_p is the P-wave reflectivity, $L_{Ipi} = \ln Z_{pi} = \ln(V_{pi} \rho_i)$ is the logarithmic P-wave impedance, and D is the difference matrix.

Fatti approximation [Fatti et al., 1994] of Aki-Richards equation [Aki and Richards, 2002] is:

$$R_{pp}(\theta) = c_{Ip}R_p + c_{Is}R_s + c_\rho R_\rho \tag{7}$$

In which
$c_{Ip} = 1 + \tan^2\theta$, $c_{Is} = -8\gamma^2\sin^2\theta$, $c_\rho = -\frac{1}{2}\tan^2\theta + 2\gamma^2\sin^2\theta$,
$\gamma = \frac{Vs}{Vp}$, and θ is the angle of incidence

$R_p = \frac{1}{2}\left(\frac{\Delta V_P}{V_P} + \frac{\Delta \rho}{\rho}\right)$, $R_s = \frac{1}{2}\left(\frac{\Delta V_s}{V_s} + \frac{\Delta \rho}{\rho}\right)$, $R_\rho = \left(\frac{\Delta \rho}{\rho}\right)$.

Substituting formula (6) into (7), the objective function 2 can be expressed by:

$$\begin{bmatrix} R_{pp}(\theta_1) \\ R_{pp}(\theta_2) \\ R_{pp}(\theta_3) \end{bmatrix} = \begin{bmatrix} c_{Ip}(\theta_1)D & c_{Is}(\theta_1)D & 2c_\rho(\theta_1)D \\ c_{Ip}(\theta_2)D & c_{Is}(\theta_2)D & 2c_\rho(\theta_2)D \\ c_{Ip}(\theta_3)D & c_{Is}(\theta_3)D & 2c_\rho(\theta_3)D \end{bmatrix} \begin{bmatrix} L_{Ip} \\ L_{Is} \\ L \end{bmatrix} \tag{8}$$

Where $L_{Ipi} = \ln Z_{pi} = \ln(V_{pi} \rho_i)$, $L_{Isi} = \ln (V_{si} \rho_i)$, and $L_{\rho i} = \ln Z_{pi} = \ln(\rho_i)$.

The low frequency content of P-, S-wave impedance and density well logs are taken the logarithm as the initial solution [Hampson, Russell, and Bankhead, 2005], and using the conjugate gradient method to gain P-, S-wave impedance and density. V_p, V_s, ρ can be then acquired after taking antilog. The inversion process is presented in Figure 2.
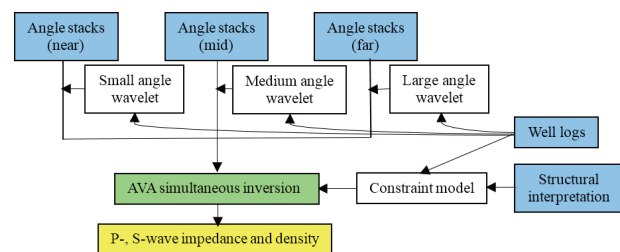

FIGURE 2. AVA simultaneous inversion process.

3.2 APPLICATION

The studied area is located in Sichuan Basin and the structure spreads to the northeast. Three angle stacks are 7-13°, 17-23°, 27-33°. The survey in Figure 3 displays the horizon.

Incorrect values of the two well-logs were removed first. Well-seismic calibration aims to estimate wavelet which is very important for seismic inversion, the quality of the wavelet directly effects the inversion result [Wang et al., 2015]. This had been done in a repeated process. A wavelet was extracted on each well and an average wavelet was calculated by the two wavelets. Three angle stacks were used in AVA simultaneous inversion so three average wavelets were computed. One of the average wavelets is shown in Figure 4 which is represented by the green line.

Well logs' band ranges from 2 to thousand Hz and are usually taken to establish low-frequency model. Low-frequency model is to constrain the inversion and supplement low frequency for seismic data [Zong et al., 2017; Zong et al., 2018]. In this inversion, P-, S-velocity and density models were established. The P-velocity model is shown in Figure 5.
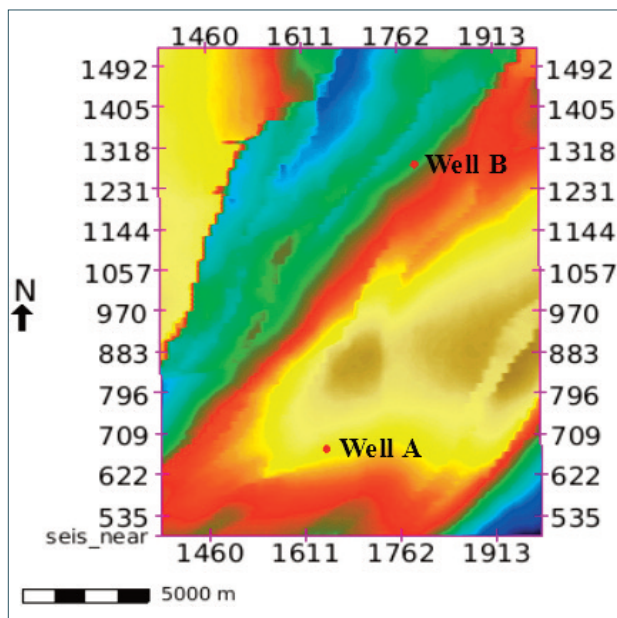
FIGURE 3. Survey of the studied area. The color shows the horizon.

4. METHODOLOGY

4.1 THE FITTING METHOD

The fitting method is actually a rock physics method. It first uses the Eaton's equation to calculate the borehole-side pore pressure. Then borehole-side pore pressure and the well log P-velocity are fitted to gain a formula, and pore pressure of the adjacent area around the well can be estimated by it. Since only two parameters that pore pressure and P-velocity are contained in the formula, the fitting method can avoid the calculation of regional NCT.

4.2 THE DIRECT CALCULATION METHOD

The direct calculation method directly uses the Eaton's equation to calculate regional pore pressure in the target layer. The LTL Formula (1) is directly used to compute the normal compaction trend. Before calculating, time-to-depth domain conversion needs to be performed to gain each point's depth. The applicable way is to use the average velocity.
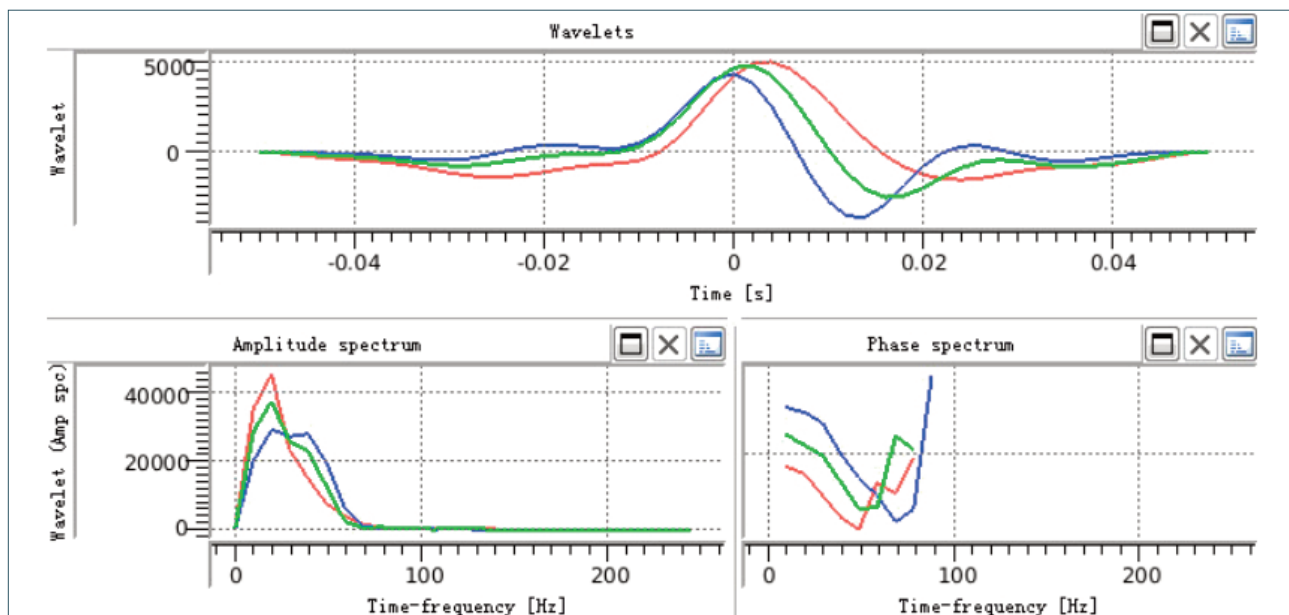

FIGURE 4. One of the average wavelets coded by green.

Parameters including V_p, V_s, ρ contrast misfit uncertainties, merge cutoff frequency, and wavelet scale factor were tested to gain the optimal estimation. Then AVA simultaneous inversion could be started. The inversion result is shown in Figure 6. The borehole-side inversion results were extracted and compared with logging curves to see how match they were, this is shown in Figure 7.

According to the comparison, P-velocity inversion result is good, but the density is not accurate. It's hard to gain satisfied density because density is insensitive to the reflectivity.

4.3 THE MODEL-BASED CALCULATION METHOD

As the aforementioned conclusion says, the NCT contributes to the pore pressure significantly. But the fitting method only computes the borehole-side NCT and omits the region's, which is a bit of careless. Besides, the horizontal continuity of the direct calculation method is poor because the NCT is computed trace by trace. There must exist constraint between traces for a set of sediments of the stratum. Ignoring this kind of constraint incurs the discontinuity, this is presented in Figure 11(a).
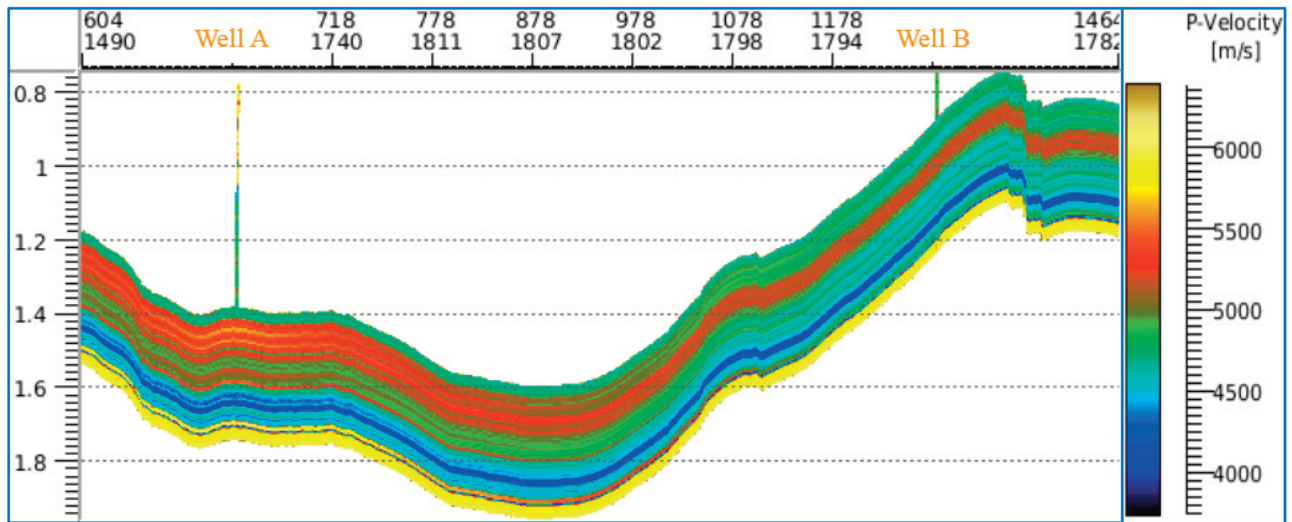
FIGURE 5. P-velocity model. Low-frequency model is to constrain inversion and supplement low frequency for seismic data.
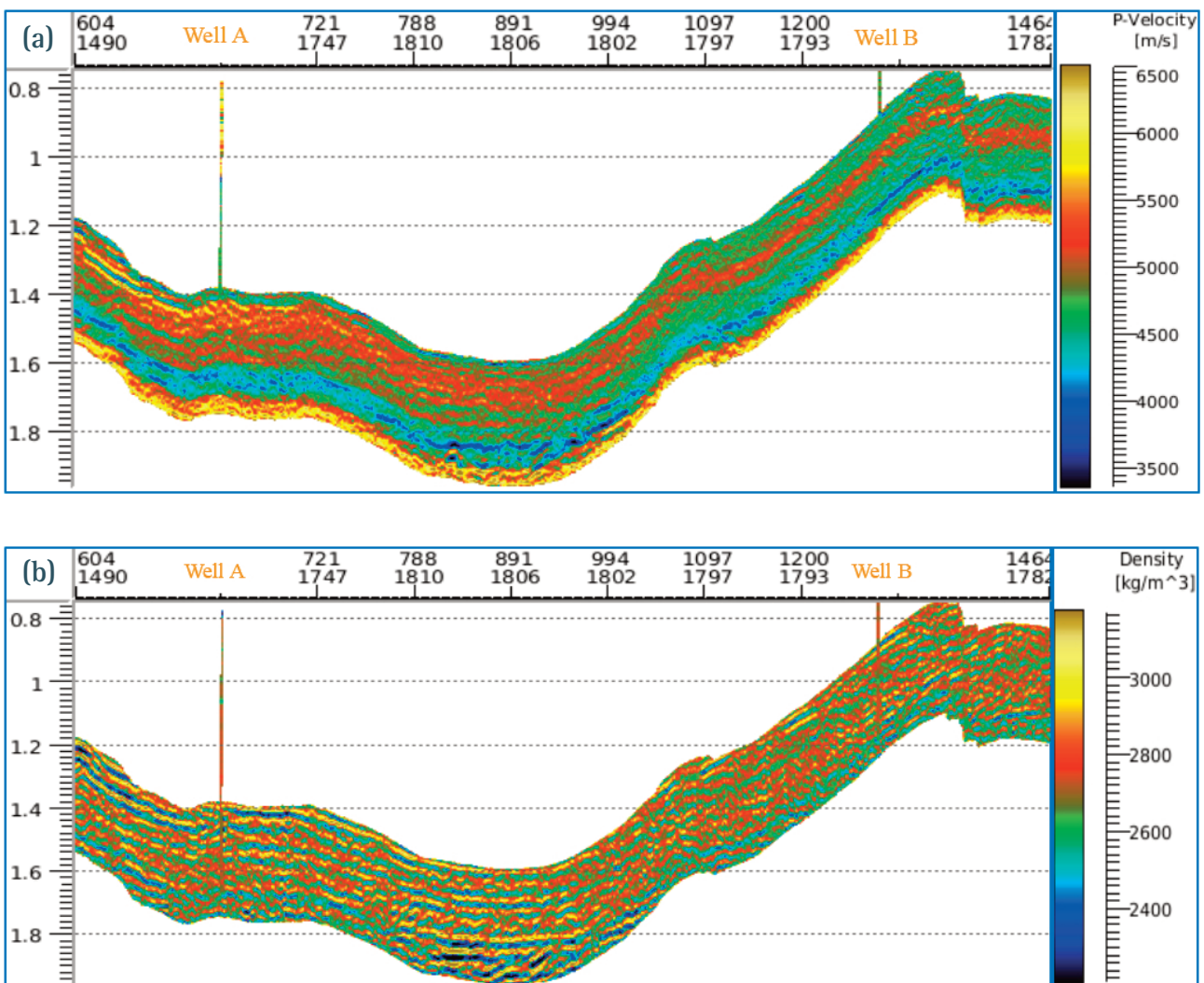

FIGURE 6. (a) P-velocity inversion result. (b) Density inversion result. AVO/AVA simultaneous inversion results.

The model-based calculation method considers the constraint. Well logs are used to construct the NCT model with an interpolation method, and then the pore pressure will be calculated by Eaton's equation. This method is applicable for the area with several wells.
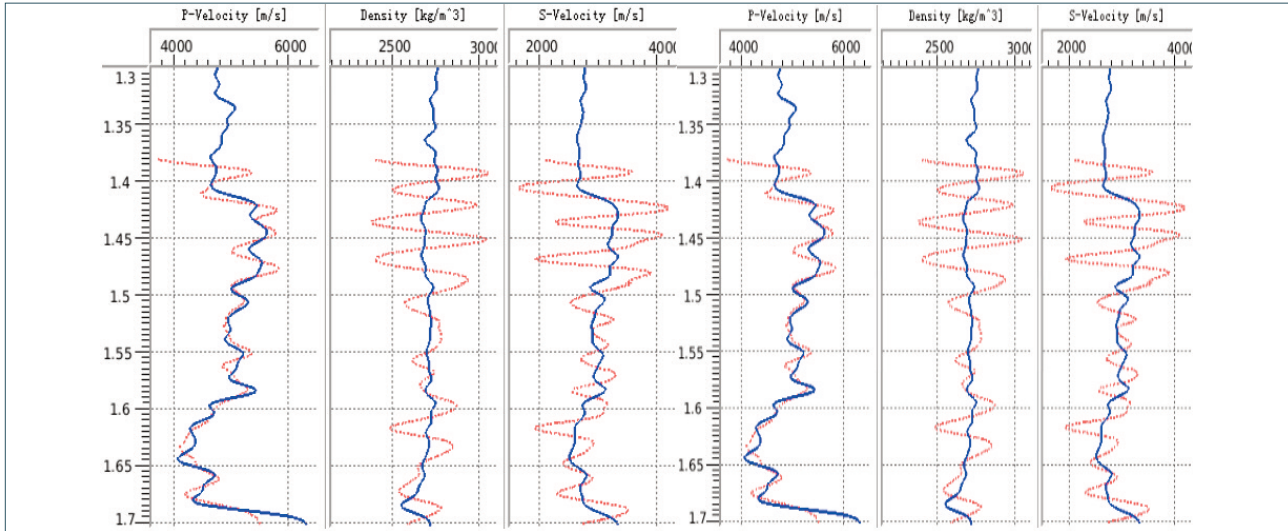
FIGURE 7. (a) Well A. (b) Well B. Comparison of well logs and the inversion result. Red dashed lines are the inversion results, and blue lines are the well logs. P-velocity matches the log well, but density is not so good. It's hard to gain satisfied density because density is insensitive to the reflectivity.
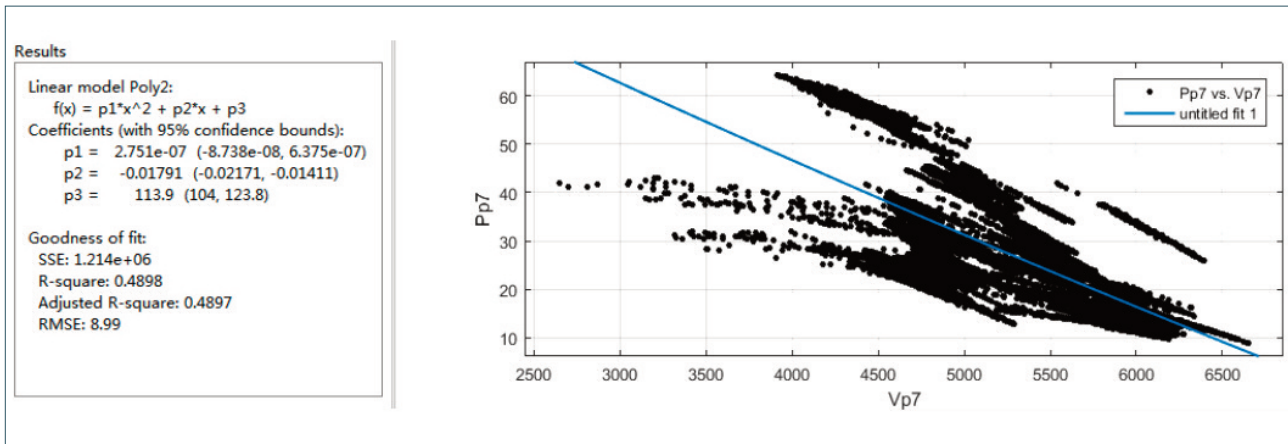

Results

Linear model Poly2:
    f(x) = p1*x^2 + p2*x + p3
Coefficients (with 95% confidence bounds):
    p1 =   2.751e-07 (-8.738e-08, 6.375e-07)
    p2 =   -0.01791 (-0.02171, -0.01411)
    p3 =   113.9 (104, 123.8)

Goodness of fit:
    SSE: 1.214e+06
    R-square: 0.4898
    Adjusted R-square: 0.4897
    RMSE: 8.99

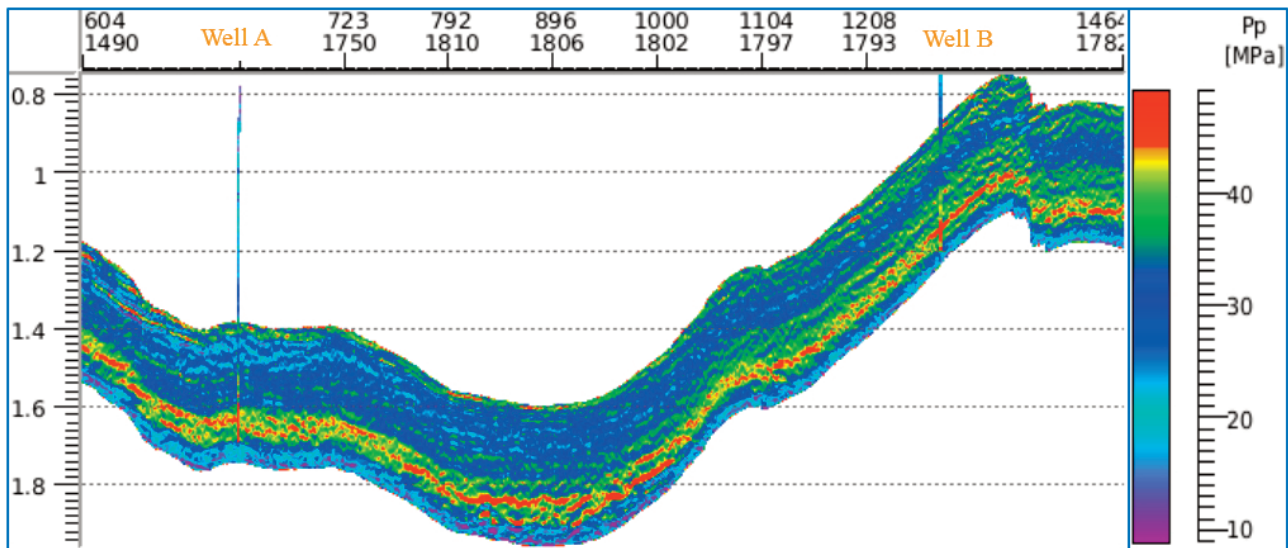**FIGURE 8.** The fit of the borehole-side pore pressure and P-velocity.

FIGURE 9. The fitting method. Pore pressure in the target layer. The fitting method only needs to estimate the borehole-side NCT, and through the fitting, calculation of regional NCT can be avoided.

5. APPLICATION AND RESULT ANALYSIS

5.1 THE FITTING METHOD

Borehole-side pore pressure was calculated with the consideration of lithology, as is shown in Figure 1 (b). The pore pressure versus P-velocity crossplot and its fit are shown in Figure 8, and the prediction result is shown in Figure 9.

The fitted formula is:

$$P_p = (2.751e-7)V_p^2 - 0.01791V_p + 113.9 \qquad (9)$$

The fitting method only needs to estimate the borehole-side NCT, and the pore pressure is calculated by the simple fitted formula, which contributes to the high efficiency.

5.2 THE DIRECT CALCULATION METHOD

The regional NCT was calculated by Formula (1), and the compaction coefficient C_1 was the average of the two wells' in the depth of the target layer, which is 0.00011. Then the pore pressure was calculated by Formula (2). The result is shown in Figure 10 (a), and the pore pressure coefficient is shown in Figure 10 (b). Pore pressure coefficient is the ratio of pore pressure to hydrostatic pressure:

$$P_c = P_p / P_n \qquad (10)$$

Where P_c is pore pressure coefficient, P_p is pore pressure, and P_n is hydrostatic pressure (i.e. normal compaction pore pressure). $P_c > 1$ indicates the overpressure, whereas $P_c < 1$ indicates the abnormal low
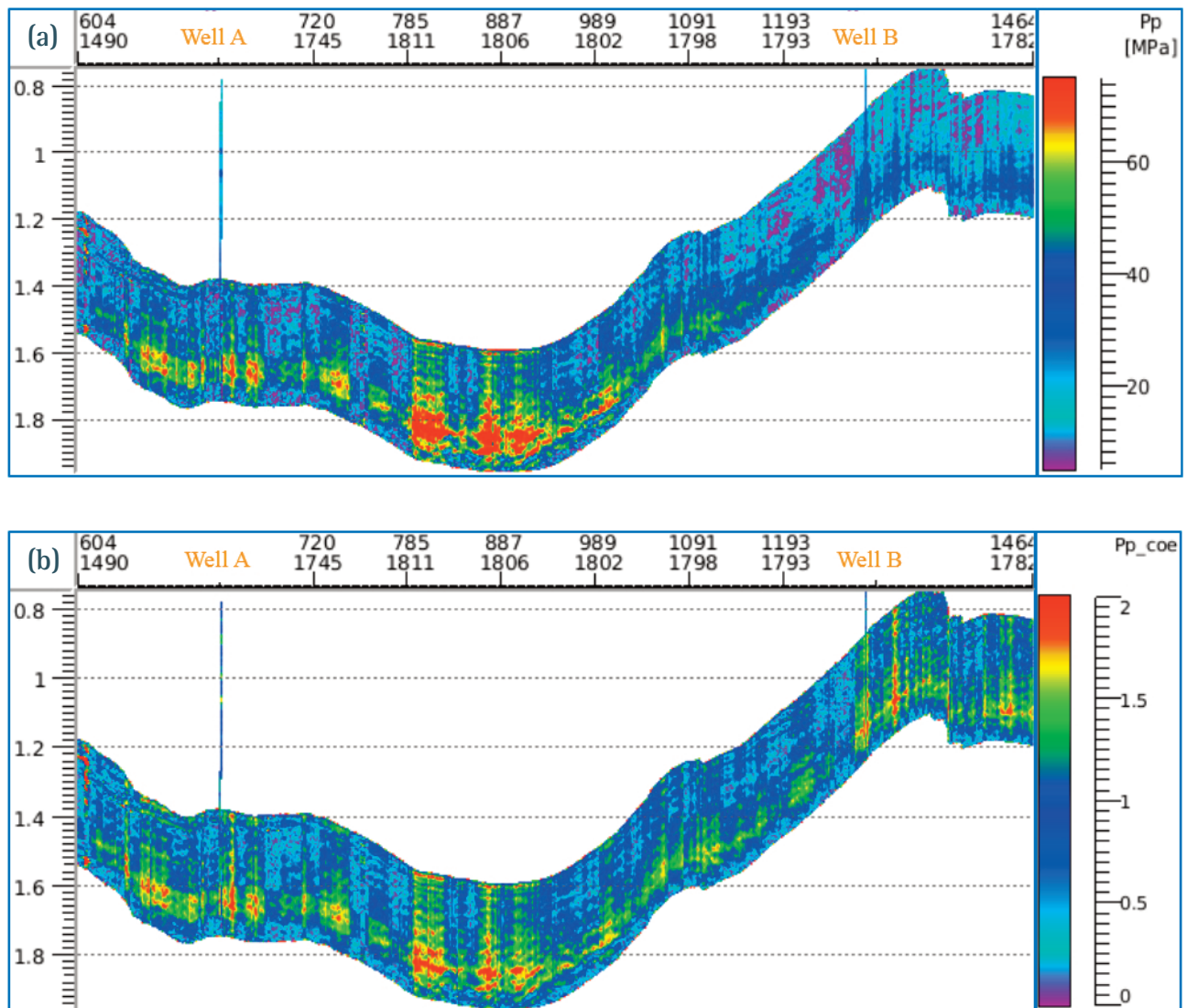

FIGURE 10. (a) The direct calculation method. Pore pressure in the target layer. Horizontal continuity is very poor, which is caused by independent computes of each trace's NCT. (b) The direct calculation method. Pore pressure coefficient in the target layer. Pressure prediction results of the direct calculation method. The Horizontal continuity is poor.
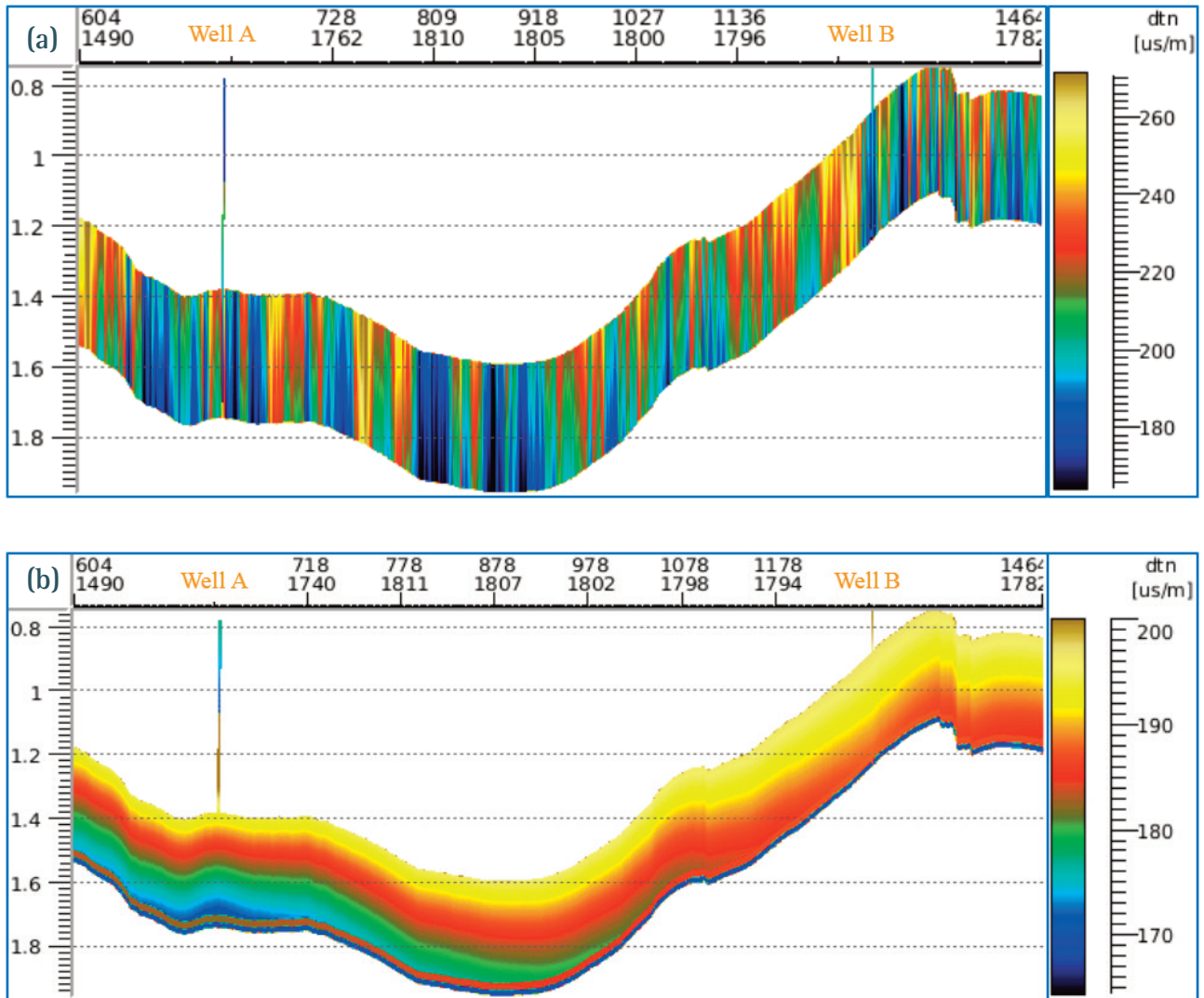
FIGURE 11. (a) The NCT of the direct calculation method. The horizontal continuity is poor, since it ignores the constraint between traces. (b) The Established NCT model. Traces between the two wells were interpolated by the Inverse Distance method. The horizontal continuity is good. Comparison of the NCT. Horizontal continuity of the direct calculation method is poor. Whereas the NCT model enhances the continuity.

pressure. It is obvious that horizontal continuity is very poor. The direct calculation method calculates each trace's NCT independently and without constraint between traces, which causes horizontal discontinuity.

5.3 THE MODEL-BASED CALCULATION METHOD

The NCT model was established with the two wells' NCT (shown in Figure 1 (b)). Traces between the two wells were interpolated by the Inverse Distance method. Figure 11 shows the comparison of the NCT in the direct calculation method and the established model. It can be seen that the established model has a very good horizontal continuity. The pore pressure and pore pressure coefficient obtained by the model-based calculation method are shown in Figure 12. The result shows an excellent horizon-

tal continuity.

Predicted pore pressures beside the borehole of the fitting method, the direct calculation method and the model-based calculation method were exacted as pseudo logs shown in Figure 13. The lest figure is the comparison of pore pressure, and the right figure is the comparison of each method's relative error. The blue medium line is the inferred borehole-side pore pressure as is shown in Figure 1 (b) (pore pressure can't be directly measured but must be inferred by quantifying the state of compaction), the black medium line is the result of the fitting method, the green small dashed line is of the direct calculation method, and the red large line is of the model-based calculation method.

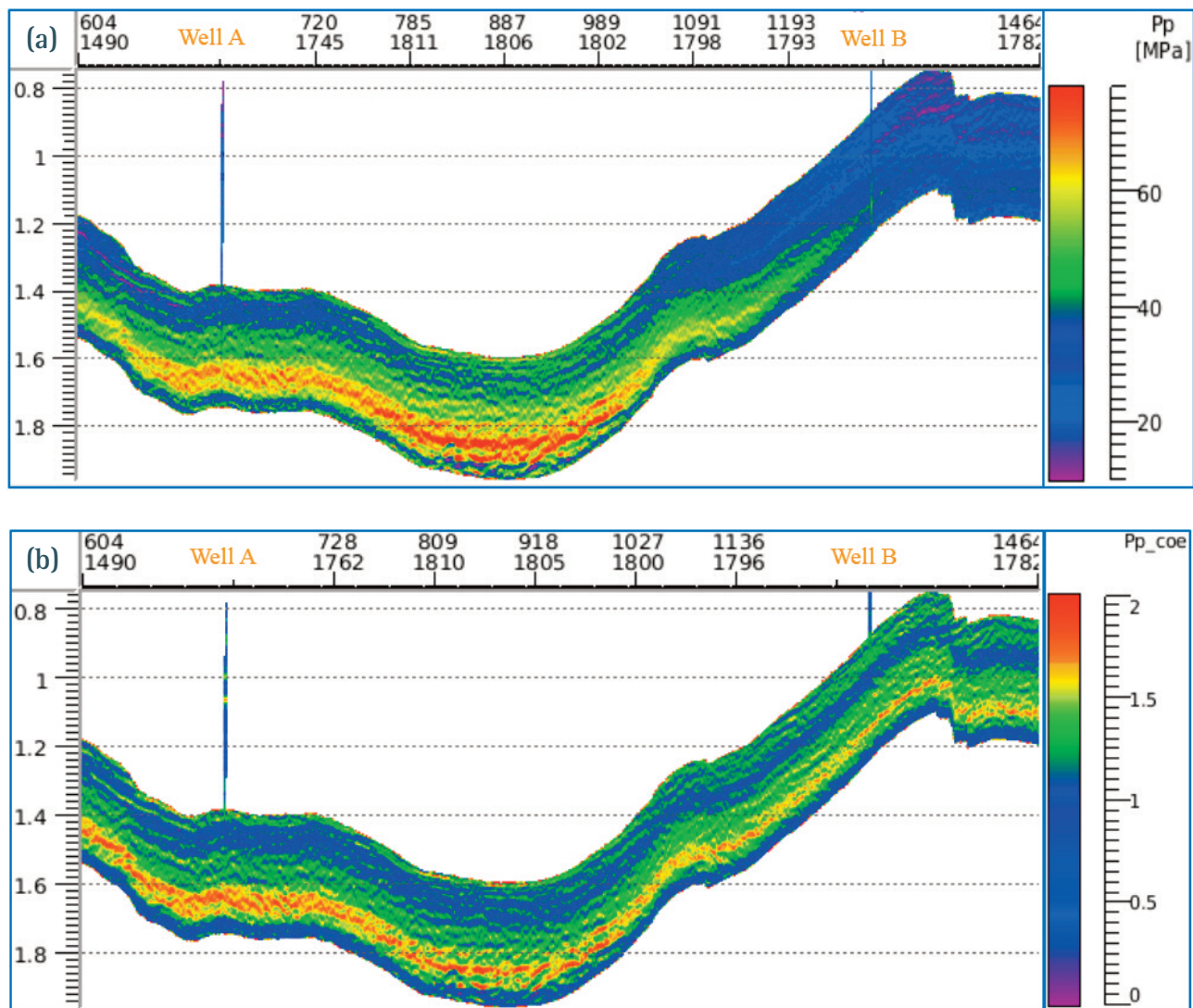The pore pressure of the model-based calculation method is the most accurate at the Well A, but is the

FIGURE 12. (a) The model-based calculation method. Pore pressure in the target layer. The horizontal continuity has a great improvement. (b) The model-based calculation method. Pore pressure coefficient in the target layer. Pressure prediction results of the model-based calculation method. The horizontal continuity has a great improvement.

lowest at the Well B. The pore pressure of the fitting method is neither good nor bad. However, the pore pressure of the direct calculation method is not good enough to be put into product. Although there is a better match than the other two methods on the Well B at the time range of 1.15 to 1.2s.

The direct calculation method directly uses the LTL to calculate the NCT, it is the easiest access to pore pressure but the precision is too low to be used. This implicates that the direct calculation of the NCT is not desirable. The fitting method is the fastest but the result is not good enough. The model-based calculation method is at both the good and the bad extremes. So in production, both the fitting method and the model-based calculation method should be performed and guide the hydraulic fracturing based on the integrated consideration.

6. CONCLUSION

Pore pressure in shale cannot be directly measured but to be inferred by the NCT. There are two elements of predicting pore pressure using Eaton's equation. One is the accurate seismic interval velocity, another is to quantify the NCT. Gain accurate seismic interval velocity has been settled, but how to precisely quantify the NCT remains unsolved.

The NCT contributes to the pore pressure a lot. When estimating the NCT, lithology must be considered to gain more reasonable and precise result. In this study, three different methods are proposed to predict pore pressure, the difference between them is how to quantify the NCT. The fitting method only bothers to calculate the borehole-side NCT and it can be regarded that the borehole-side NCT is took to rep-
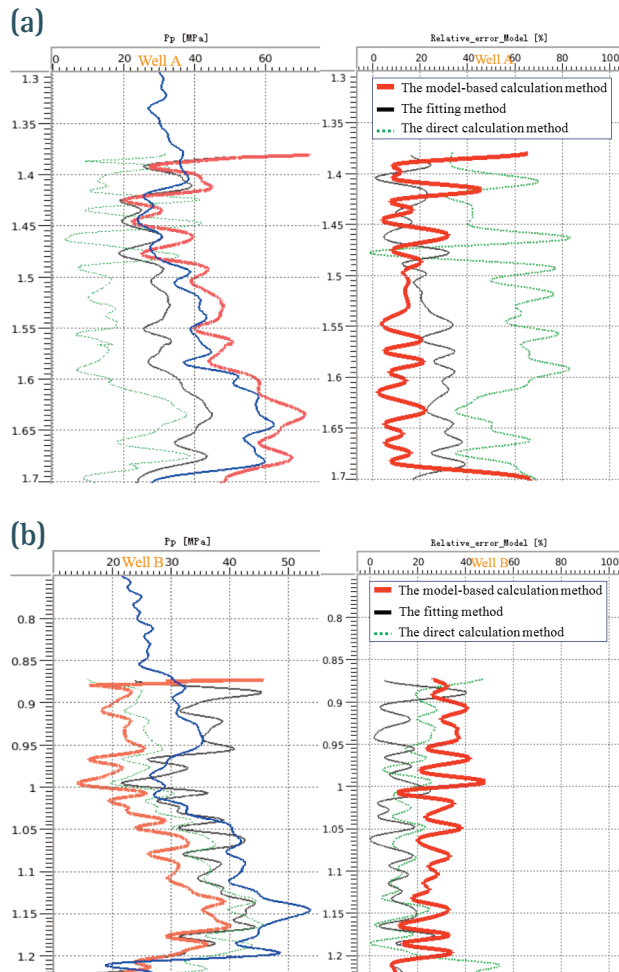
(a)

(b)

FIGURE 13. (a) Comparison of well A's result. The left is the comparison of pore pressure, and the right is the comparison of each method's relative error. The relative error of the model-based calculation method is the smallest, which is about 11%. (b) Comparison of well B's result. The left is the comparison of pore pressure, and the right is the comparison of each method's relative error. The relative error of the fitting method is the smallest, which is about 10%. Comparison of the borehole-side result. Blue medium line is the inferred borehole-side pore pressure, the black medium line is the result of the fitting method, the green small dashed line is of the direct calculation method, and the red large line is of the model-based calculation method.

resent the region's. This method has the highest efficiency, and the accuracy is at a medium level. The direct calculation method is the easiest. This method directly calculates the regional NCT by the LTL, but the precision of the pore pressure is too low to be used, which implicates that the direct calculation of the NCT is not desirable. The model-based calculation method estimates the regional NCT by constructing the NCT model, and the accuracy of the result is at two extremes. It is suggested that both the fitting method and the model-based calculation method be integratedly used in practice.

Besides, the result also shows that the different approach of quantifying the NCT impacts the horizontal continuity significantly. The direct calculation method calculates each trace's NCT independently, and the result shows awful horizontal continuity. Whereas, the model-based calculation method considers the constraint with the interpolation method and gets a better estimation. When computing the NCT, the constraint between traces must be taken into account.

REFERENCES

Aishan, L., Xingyao, Y., Fanchang, Z., and Baoli, W. (2007). Application of prestack simultaneous AVA multi-parameter inversion in gas-bearing reservoir prediction. Geophysical Prospecting for Petroleum, 46(1), 64.

Aki K., and P. G. Richards (2002). Quantitative seismology, 2nd Edition: W. H. Freeman and Company.

Brian Russell and Dan Hampson (1991). Comparison of poststack seismic inversion methods. SEG Technical Program Expanded Abstracts, 876-878.

Debeye, H. W. J., and RIEL, V. P. (1990). Lp NORM DE-CONVOLUTION. Geophysical Prospecting, 38(4), 381-403.

Eaton, B. A. (1972). The effect of overburden stress on geopressure prediction from well logs. Journal of Petroleum Technology, 24(08), 929-934

Eaton, B. A. (1975). The equation for geopressure prediction from well logs. In Fall meeting of the Society of Petroleum Engineers of AIME. Society of Petroleum Engineers.

Fatti, J. L., Smith, G. C., Vail, P. J., Strauss, P. J., and Levitt, P. R. (1994). Detection of gas in sandstone reservoirs using AVO analysis: A 3-D seismic case history using the Geostack technique. Geophysics, 59(9), 1362-1376.

Fillippone, W. R. (1982). Estimation of formation parameters and the prediction of overpressures from seismic data. In 1982 SEG Annual Meeting. Society of Exploration Geophysicists.

Foster, J. B. (1966). Estimation of formation pressures from electrical surveys-Offshore Louisiana. Journal of Petroleum Technology, 18(02), 165-171.

Gutierrez, M. A., Braunsdor, N. R., and Couzens, B. A. (2006). Calibration and ranking of pore-pressure prediction models. The Leading Edge, 25(12), 1516-1523

Hampson, D. P., Russell, B. H., and Bankhead, B. (2005, January). Simultaneous inversion of pre-stack seismic data. In 2005 SEG Annual Meeting. Society of Exploration Geophysicists.

Han, T., Pervukhina, M., Ben Clennell, M., and Neil Dewhurst, D. (2017). Model-based pore-pressure prediction in shales: An example from the Gulf of Mexico, North America. Geophysics, 82(3), M37-M42

Hong, G. (2008). Formation pressure prediction with well constrained seismic inversion: A case from A Sag in Bohai Bay Basin. Natural Gas Geoscience, 19(2), 276-279.

Hottmann, C. E., and Johnson, R. K. (1965). Estimation of formation pressures from log-derived shale properties. Journal of Petroleum Technology, 17(06), 717-722.

King Hubbert, M., and Rubey, W. W. (1959). Role of fluid pressure in mechanics of overthrust faulting: I. Mechanics of fluid-filled porous solids and its application to overthrust faulting. Geological Society of America Bulletin, 70(2), 115-166.

Law, B. E., and Spencer, C. W. (1998). Memoir 70, Chapter 1: Abnormal Pressure in Hydrocarbon Environments.

Ma, X. Q. (2002). Simultaneous inversion of prestack seismic data for rock properties using simulated annealing. Geophysics, 67(6), 1877-1885.

Meissner, F. F. (1981). Abnormal pressures produced by hydrocarbon generation and maturation and their relation to processes of migration and accumulation. AAPG Bulletin, 65(11), 2467-2467.

Peter, V. R., Richard, H., and Peter, T. (2004). The origin of overpressure in the Carnarvon Basin. Western Australia: Implications for pore pressure prediction: Petroleum Geoscience, 10, 247-257.

Serebryakov, V. A., Robertson Jr, J. O., and Chilingarian, G. V. (Eds.) (2002). Origin and prediction of abnormal formation pressures (Vol. 50). Gulf Professional Publishing.

Sviridov, V. A., Mayr, S. I., and Shapiro, S. A. (2017). Elastic properties of two VTI shale samples as a function of uniaxial stress: Experimental results and application of the porosity-deformation approach. Geophysics, 82(6), C201-C210.

Tingay M.R.P., Hillis R.R., Swarbrick R.E., Morley C.K., Damit A.R. (2009). Origin of overpressure and pore-pressure prediction in the Baram province, Brunei.

AAPG Bull, 93 (1), 51–74.

Tissot, B. P., and Welte, D. H. (1984). Locating Petroleum Prospects: Application of Principle of Petroleum Generation and Migration—Geological Modeling. Petroleum Formation and Occurrence. Springer Berlin Heidelberg: 571-582.

Wang, S., Yuan, S., Ma, M., Zhang, R., & Luo, C. (2015). Wavelet phase estimation using ant colony optimization algorithm. Journal of Applied Geophysics, 122, 159-166.

Wang, X., Wu, S., Xu, N., and Zhang, G. (2006). Estimation of gas hydrate saturation using constrained sparse spike inversion: Case study from the northern South China Sea. Terrestrial Atmospheric and Oceanic Sciences, 17(4), 799.

Yang W.Y. (2010). Prestack simultaneous AVA inversion algorithm with simulated annealing. Progress in Geophysics, 25(1):219-224.

Yuan, S., Wang, S., Luo, C., and He, Y. (2015). Simultaneous multitrace impedance inversion with transform-domain sparsity promotion. Geophysics, 80(2), R71-R80.

Zhang, J. (2011). Pore pressure prediction from well logs: Methods, modifications, and new approaches. Earth-Science Reviews, 108(1-2), 50-63.

Zong Zhaoyun and Yin Xingyao. (2017). Model parameterization and p-wave AVA direct inversion for Young's impedance. Pure and Applied Geophysics, 174(5): 1965–1981.

Zong Zhaoyun, Wang Yurong, Li Kun, Yin Xingyao. (2018). Broadband Seismic Inversion for Low-Frequency Component of the Model Parameter. IEEE Transactions on Geoscience & Remote Sensing, 99:1-8.

Zong Zhaoyun, Yin Xingyao, Wu Guochen et al. (2017). Broadband seismic amplitude variation with offset inversion. Geophysics, 82(3): M43-M53.

*CORRESPONDING AUTHOR: Ting LEI,
School of Geosciences, China University of Petroleum (Huadong),
Qingdao, China.

email: Leiting0571@qq.com